HHS Public Access

Author manuscript

Phys Med Biol. Author manuscript; available in PMC 2016 April 21.

Published in final edited form as:

Phys Med Biol. 2015 April 21; 60(8): 3111–3127. doi:10.1088/0031-9155/60/8/3111.

Optimization of Multi-Pulse Sequences For Nonlinear Contrast Agent Imaging Using a cMUT Array

Anthony Novell, **Christopher B. Arena**, **Sandeep Kasoji**, and **Paul A. Dayton**

Joint Department of Biomedical Engineering, The University of North Carolina and North Carolina State University, Chapel Hill, NC 27599, USA

Abstract

Capacitive micromachined ultrasonic transducer (cMUT) technology provides advantages such as wide frequency bandwidth, which can be exploited for contrast agent imaging. Nevertheless, the efficiency of traditional multi-pulse imaging schemes, such as pulse inversion (PI), remains limited because of the intrinsic nonlinear character of cMUTs. Recently, a new contrast imaging sequence, called bias voltage modulation sequence (BVM), had been specifically developed for cMUTs to suppress their unwanted nonlinear behavior. In this study, we propose to optimize contrast agent detection by combining the BVM sequence with PI and/or chirp reversal (CR). An aqueous dispersion of lipid encapsulated microbubbles was exposed to several combinations of multi-pulse imaging sequences. Approaches were evaluated *in vitro* using 9 inter-connected elements of a cMUT linear array (excitation frequency of 4 MHz; peak negative pressure of 100 kPa). For sequences using chirp excitations, a specific compression filter was designed to compress and extract several nonlinear components from the received microbubble responses. A satisfactory cancellation of the nonlinear signal from the source is achieved when BVM is combined with PI and CR. In comparison with PI and CR imaging modes alone, using sequences incorporating BVM increases the contrast-to-tissue ratio by 10.0 dB and 4.6 dB, respectively. Furthermore, the combination of BVM with CR and PI results in a significant increase of the contrast-to-noise ratio (+29 dB). This enhancement is attributed to the use of chirps as excitation signals and the improved preservation of several nonlinear components contained within the contrast agent response.

Keywords

Bias voltage; chirp; cMUT; contrast agent; microbubbles; multi-pulse sequence; nonlinearity

I. INTRODUCTION

Contrast enhanced ultrasound involves the systemic administration of shelled, gas-filled microbubbles into the vascular space via intravenous injection. Microbubbles are highly echogenic, and are used to improve ultrasound backscatter and signal strength in well-vascularized regions of tissue typically characterized by poor image contrast. This aids in

Corresponding author: Paul A. Dayton, PhD., Joint Department of Biomedical Engineering, The University of North Carolina and North Carolina State University, CB7575, Chapel Hill, NC 27599, USA, Tel: 919 843 9519, padayton@email.unc.edu.

the characterization of several disease states that can be linked to alterations in blood perfusion, including coronary artery disease (Mulvagh *et al* 2000), kidney disease (Ignee *et al* 2010), and cancer (Wilson and Burns 2010, Novell *et al* 2013b). Multiple commercial microbubble formulations exist, the most common of which include SonoVue® (sulphur hexafluoride core, surfactant shell), Optison™ (octafluoropropane core, albumin shell), and DEFINITY™ (octafluoropropane core, lipid shell).

When insonified at low pressures, tissue reflects acoustic waves primarily at the same frequency that was transmitted (linear fundamental component, f_0). Microbubbles, on the other hand, oscillate nonlinearly and produce echoes with a greater proportion of higher order harmonics and sub-harmonics (Frinking *et al* 2000, de Jong *et al* 2002). Conventional contrast agent imaging schemes utilize this fact in order to isolate backscattered signals from microbubbles and suppress tissue signals. For example, in contrast harmonic imaging, bandpass filtering is applied around certain harmonics (*e.g.*, $0.5f_0$ (Chomas *et al* 2002), $2f_0$ (de Jong *et al* 2002), $3f_0$ or more (Bouakaz *et al* 2002, Gessner *et al* 2013)) in order to enhance microbubble specificity (contrast-to-tissue ratio, CTR). Second harmonic imaging is commonly used for contrast agent imaging because this harmonic component is often the strongest. However, this technique becomes challenging at high pressures (mechanical index ≥ 0.3), as the transmit wave is distorted due to nonlinear propagation and contains harmonics that are scattered linearly by tissue and mask microbubble signals (Hamilton and Blackstock 1998). Consequently, low transmit pressures are required to preserve the specificity at the cost of sensitivity (contrast-to-noise ratio, CNR).

To further improve the CTR, multi-pulse sequences, such as pulse inversion (PI (Simpson *et al* 1999)) and power modulation (PM (Brock-Fisher *et al* 1996)), have been implemented. These techniques combine the received signals from multiple, unique transmit pulses, such that there is cancellation of the linear fundamental response and preservation of nonlinear content. Researchers have also shown that there is benefit to combining PI and PM (PIPM). Eckersley *et al.* reported a 4 dB increase in microbubble response using PIPM when compared to PI or PM alone (Eckersley *et al* 2005). In PIPM, the nonlinear components from PI and the nonlinear components from PM (which are distinct) are added together to improve the signal strength. Another variation of PIPM, known as cadence contrast pulse sequence (CPS) was shown to increase microbubble response while also eliminating tissue motion artifacts (Phillips 2001).

The sequences mentioned above use transmit pulses with a single carrier frequency. Recently, chirp signals have been investigated, which consist of multiple sinusoidal cycles of increasing (up-chirp) or decreasing frequency (down-chirp) (O'Donnell 1992, Misaridis *et al* 2000, Song *et al* 2011, Park *et al* 2013, Maresca *et al* 2013). Chirps allow for the delivery of additional energy into the tissue (in the form additional cycles) that increases both the penetration depth and the intensity of backscattered echoes, at the expense of the axial resolution. In order to recover the axial resolution, pulse compression must be implemented by performing cross-correlation between the transmit chirp and received echoes (Misaridis and Jensen 2005). Previous studies have reported the potential of chirps for contrast subharmonic or harmonic imaging (Borsboom *et al* 2005, Zhang *et al* 2007, Shekhar and Doyley 2013). A multi-pulse sequence that utilizes chirps, and exploits the

nonlinear resonance behavior of microbubbles has been developed by Novell *et al.* (Novell *et al* 2009b). In this technique, called chirp reversal (CR), echoes from an up-chirp and down-chirp were combined to isolate the nonlinear response to microbubbles. By transmitting the up-chirp first, and the down-chirp second, differences in terms of length and amplitude of microbubble responses can be observed. This additional energy was transformed into improved signal strength following pulse compression. The authors later showed that, like PIPM, CR can be combined with PM to further increase CTR and CNR (3dB increase in microbubble response compared to CR or PM alone) (Novell *et al* 2014b).

In the past, CR and CRPM have been performed using traditional piezoelectric transducers (Novell *et al* 2014b). While successful at improving the signal strength from microbubbles, the narrow frequency bandwidth of piezoelectric transducers only excites microbubbles with a resonant frequency near the center frequency of the transducer; this represents a small fraction of the entire microbubble population. We hypothesize that a broader range of microbubbles sizes may be excited during the up-chirp and down-chirp by using a capacitive micro-machined ultrasonic transducer (cMUT), and that this may lead to added gains in CNR and CTR. cMUT's potential for wideband contrast agent imaging has been already demonstrated by Novell *et al*. (Novell *et al* 2013a). cMUTs consist of a series of interconnected, flexible membranes surrounded by activation electrodes. An AC voltage is applied across the electrodes in order to generate an electrostatic force, which leads to membrane vibrations and the generation of acoustic waves. cMUTs are known for having a wide frequency bandwidth (Huang *et al* 2006, Savoia *et al* 2012, Novell *et al* 2013a) and are currently under development in the field of ultrasound for Doppler imaging (Shin *et al* 2013), intravascular ultrasound (Tekes *et al* 2012), photoacoustic imaging (Vaithilingam *et al* 2009, Chen *et al* 2012) and high-intensity focused ultrasound (Bayram *et al* 2005, Wong *et al* 2010).

In order to successfully perform multi-pulse contrast imaging with cMUTs, it is first necessary to account for their inherent nonlinear behavior that causes harmonic content to be transmitted masking the nonlinear responses from microbubbles (Lohfink and Eccardt 2005b). This nonlinear behavior mainly arises from the dependence of electrostatic force on the square of the excitation voltage. Several feasible methods for eliminating the unwanted harmonic content have recently been developed (Zhou *et al* 2004, Satir and Degertekin 2012, Novell *et al* 2009a). Very recently, Novell *et al.* have proposed a new multi-pulse scheme based on bias voltage modulation (BVM) that enhances nonlinear contrast agent response while suppressing the harmonics emitted by the cMUT (Novell *et al* 2014a). For proper cMUT operation, a DC bias voltage is applied across the electrodes in order to improve the sensitivity. BVM combines the received echoes from three transmit pulses with varying bias voltages (e.g., 20 V, 40 V, and 60 V) in order to cancel the signals from linear reflectors (i.e., tissue) while maintaining the signals from microbubbles. A CTR increase of 17 dB was achieved when the BVM sequence was compared independently to second harmonic imaging; a 6 dB increase was achieved compared to PM (Novell *et al* 2014a).

BVM was originally developed to adapt the well-established power modulation (PM) sequence to cMUT array transducer technology. Previous results demonstrated that a complete cancellation of the nonlinear signal from the source could be accomplished when

the BVM sequence was implemented (Novell *et al* 2014a). Nevertheless, the efficiency of other multi-pulse approaches based on nonlinear detection processes, such as PI and CR, remains limited by the cMUT nonlinear behavior. Moreover, as previously reported in (Phillips 2001, Eckersley *et al* 2005, Novell *et al* 2014b), the combination of several approaches (e.g., PIPM, CRPM) increased the sensitivity for detecting nonlinear responses from microbubbles. In this context, our objective in this paper was to combine the BVM sequence with these approaches to (i) suppress the undesirable harmonic component generated by the cMUT, (ii) optimize contrast agent detection.

II. MATERIAL AND METHODS

A) Contrast agent preparation

Polydisperse octafluoropropane microbubbles were formulated by dissolution of 1,2-distearoyl-*sn*-glycero-3-phosphocholine (DSPC) and 1,2-distearoyl-sn-glycero-3-phosphoethanolamine-N-methoxy(polyethylene-glycol)-2000 (DSPE-PEG2000) in a 9:1 molar ratio and a total lipid concentration of 1.0 mg/mL as previously described (Mullin *et al* 2011). Lipids were purchased from Avanti Polar Lipids (Alabaster, AL, USA). The excipient solution was comprised of phosphate-buffered saline (PBS), propylene glycol, and glycerol (16:3:1). 1.5 mL of the resulting solution was pipetted into a 3 mL glass vial and gas exchanged with octofluoropropane (FluoroMed, Round Rock, TX, USA) to replace the free and dissolved air. This formulation is similar to that of DEFINITY®, which has been FDA approved for echocardiography. A Vialmix shaker (Bristol-Myers-Squibb, New York, NY) was used to generate microbubbles via mechanical agitation. An AccuSizer 780A (Particle Sizing Systems, Port Richey, FL, USA) was used to quantify the population of microbubbles. The averaged distribution of microbubbles had a mean diameter of 1.0 ± 0.6 μm and a total concentration of $8.0 \times 10^{10} \pm 3.3 \times 10^{9}$ bubbles/mL.

B) Ultrasound multi-pulse sequences

Gaussian apodized sinusoidal burst signals (x_p) centered at 4 MHz were transmitted for monochromatic excitation sequences (*i.e.*, PI, BVM, BVMPI). A fractional bandwidth at −6 dB of 42% was chosen to avoid the frequency band overlapping between the fundamental and 2nd harmonic components. This separation of the two frequency components was required to assess the contribution of each multi-pulse sequence on the generation of nonlinear responses. Nevertheless, the multi-pulse approaches described in this paper remained suitable for wide band pulses traditionally used for imaging (bandwidth > 60%). Linear frequency modulated chirp signals centered at f_c = 4 MHz were used for approaches based on CR. Gaussian apodized chirps with a frequency modulation of $\frac{\Delta f}{\Delta t} = \frac{2}{4} \frac{MHz}{\mu s}$ were transmitted in order to obtain a similar bandwidth (*i.e.*, 42%) to sinusoidal burst excitations (x_p). As defined in the CR sequence, the down-sweep frequency chirp (x_{dnf}) is the time-reversed replica of the up-sweep frequency chirp (x_{upf}). A list of the transmitted excitations (s_i) as a function of the contrast imaging sequence is given in Table I. For sequences based on BVM, the transmission of at least three firings at different bias voltages (V_{dc}= 30 V, 60 V, and 90 V) were necessary. For comparison, PI and CR were performed at V_{dc}= 90V to achieve the best sensitivity. Because the nonlinear cMUT behavior depended

on the transmitted frequency, the combination of BVM with CR was challenging and required optimization. For this reason, a fourth firing was transmitted for methods combining BVM and CR. This issue is described in further detail later in the paper (Discussion section and Figure 7).

The axial resolution was recovered by correlating the receive echo signal with a specific compression filter. In the case of BVM and CR strategies, the recovery of more than one frequency component (*e.g.*, f_0, $2f_0$) improves contrast agent detection (Novell *et al* 2014b, Novell *et al* 2014a). Because the compression filter acts as a bandpass filter, it must be optimized for nonlinear contrast imaging. For this reason and as previously described in (Novell *et al* 2014b), the compression filter was composed of the sum of two chirps: one identical to the excitation signal (*i.e.*, x_{upf} or x_{dnf}) centered at the fundamental frequency f_0 and another centered at the $2f_0$ frequency to extract both the fundamental and the harmonic components. The frequency modulation of the $2f_0$ component was also equal to

$$\frac{\Delta f}{\Delta t} = \frac{2 \quad MHz}{4 \quad \mu s}.$$

For each contrast imaging sequence, the received signals from the multiple firings were combined to extract nonlinearities from the interrogated medium (*e.g.*, microbubbles). The post-processing operations used in this study to extract contrast agent responses are given in Table II where E_i is the backscattered signal (after compression in the case of chirp excitations) from s_i. For all methods based on BVM approach, weighting factors were specifically chosen to suppress the linear reflection resulting from both the fundamental and the undesirable 2nd harmonic components generated by the source (Novell *et al* 2014a). Furthermore, the weighting factors were normalized in order to compare the contrast enhancement resulting from each imaging sequence. Consequently, differences observed in terms of sensitivity could not be attributed to a change in the number of firings.

C) cMUT probe specifications

Multi-pulse sequences were evaluated using a prototype cMUT probe (Vermon SA, Tours, France) centered at 6.5 MHz. The design of the prototype probe was limited to 9-inteconnected elements, with a pitch of 205 μm and an elevational aperture of 5 mm. Elements were interconnected to generate a plane wave with a sufficient amplitude (*i.e.*, the amplitude of the output wave should be high enough to induce a nonlinear response from microbubbles). The static collapse voltage of the probe (140V) and the fractional bandwidth at −3 dB (81%) were estimated by hydrophone measurements (HNA-0400, Onda Corp., Sunnyvale, CA, USA).

D) Apparatus

Gaussian apodized sinusoidal burst excitations (x_p) and Gaussian chirp excitations (x_{upf} *or* x_{dnf}) were designed using Matlab (release 2009A, The Mathworks, Natick, MA, USA) and then transferred to an arbitrary waveform generator (AFG 3101, Tektronix, Beaverton, OR, USA) through a GPIB connection (National Instruments, Austin, TX, USA). Signals were then amplified with a 60 dB power amplifier (A-500, ENI, Rochester, NY, USA) and transmitted to the cMUT probe. The amplitude of the excitation voltage (v_{ac}) was fixed at 75

V_{pp} during the rest of the study. The desired bias voltage (*i.e.*, 30 V, 60 V or 90 V) was delivered using a controllable power supply (Model 9185, B&K Precision, Yorba Linda, CA, USA) according to the required bias of the specific imaging sequence. For each transmitted signal, the acoustic wave generated by the cMUT was measured at 20 mm from the face of the transducer using a calibrated hydrophone. A/D conversion was performed at a sampling rate of 100 MHz using a 14-Bit waveform digitizer (PDA14, Signatec, Lockport, IL, USA) controlled by LabVIEW (National Instruments, Austin, TX, USA) to visualize and record the received signals on a personal computer.

E) Simulations

The interest of combining PI and/or CR with BVM to improve the detection of a simulated response of a single microbubble was evaluated. The acoustic response of 1.3 μm radius microbubble was calculated using a modified Rayleigh-Plesset equation (de Jong *et al* 1994). The shell parameters given by Goertz *et al.* (Goertz *et al* 2007) were used to simulate a DEFINITY microbubble. The microbubble resonance frequency corresponded to the excitation frequency (*i.e.*, f_c = 4 MHz). For each of three pulses, the acoustic waveform measured 20 mm from the cMUT output was introduced into the equation as the driving signal. Pressure amplitudes measured from hydrophone measurements (*i.e.*, peak negative pressures of 35 kPa, 67 kPa and 100 kPa for a bias voltage of 30V, 60V and 90V, respectively) were used to excite the simulated microbubble.

F) In vitro measurements

Two sets of *in vitro* experiments were performed in order to evaluate the efficiency of the imaging sequences. First, a solution of diluted microbubbles (dilution factor of 1:150 in PBS) was injected in a stand-alone microcellulose tube (212 μm outer diameter) immersed in a water tank. Prior to microbubble experiments, the tube was filled with air to be positioned 20 mm from the cMUT probe using a pulse-echo measurement. The receive sensitivity of the 9-element cMUT array was insufficient for extracting a satisfactory response from microbubbles. Consequently, received signals were acquired using a 7.5 MHz single-element piezoelectric transducer (1.27 cm diameter, 66% bandwidth at −6 dB; V320, Panametrics Inc., Waltham, MA, USA). Using a 3D motion controller (Model XPS, Newport Corporation, Irvine, CA, USA), the receive transducer was placed perpendicularly to the cMUT probe to avoid any reflection and 5 cm (corresponding to its focal distance) from the tube. Received signals were amplified (20 dB) using a broadband receiver (BR-640A, RITEC Inc., Warwick, RI, USA) before being converted and transferred to a personal computer. The different excitation signals required for each of the imaging sequences (Table I) were successively transmitted with a delay of 1s. This delay was limited by the time to transfer the desired waveform into the function generator. For each sequence, contrast enhancement and CNR were calculated by averaging 10 individual measurements. Between each measurement, fresh microbubbles were infused for 30 seconds at a flow rate of 100 $\mu l.min^{-1}$ using a syringe pump (PHD2000, Harvard Apparatus, Holliston, MA, USA). The flow of microbubbles was stopped 30 seconds prior to measurements to ensure that the same population of microbubbles was interrogated by the diverse firings defined in the multi-pulse sequence. The experiment was repeated three times using microbubbles from different vials to examine batch-to-batch variance in the microbubble population. Statistical

analysis was performed using the Mann-Whitney-test using the software StatPlusmac 2009 (AnalystSoft, Vancouver, Canada). A p-value <0.05 was considered as statistically significant. The noise level was obtained by performing the same experiment without any scatterers present within the tube. Similarly, echoes from a solid reflector (silver wire 100 μm diameter) were recorded for each transmit pulse in order to assess the ability of the different multi-pulse sequences in suppressing linear reflections (at f_0 and $2f_0$).

In the second set of experiments, the microcellulose tube was embedded in a tissue mimicking phantom immersed in a water bath as shown in Figure 1a. The dimensions of the phantom are given in Figure1b. The base material of the phantom was similar to that described in (King *et al* 2011), except that graphite powder (13.5 g) was used as the scattering medium. The other components of the recipe (gellan gum, calcium chloride, potassium sorbate, and propanol) and their proportions remained the same. The attenuation coefficient of the phantom was estimated for frequencies ranging from 1 MHz to 8 MHz using the through-transmission substitution technique (Madsen *et al* 1999). The ultrasound attenuation exhibited a frequency dependent relationship as $\alpha(f) = Af^n$ where $A = 0.24 \pm 0.02$ $dB.cm^{-1}.MHz^{-1}$ and n = 1.46. This attenuation coefficient was on the same order of magnitude as typical attenuation values measured for blood (0.09-0.17 $dB.cm^{-1}.MHz^{-1}$) and fatty tissue (0.38-0.78 $dB.cm^{-1}.MHz^{-1}$) (Pohlhammer and O'Brien 1980). Imaging sequences were applied using the same protocol previously described for the stand-alone tube experiments.

III. RESULTS

A) Hydrophone measurements

Hydrophone measurements were performed to evaluate the transmitted pressure amplitude and the degree of nonlinearity generated by the cMUT. Figure 2 shows the results for a Gaussian apodized sinusoidal burst (left column) and an up-sweep frequency chirped pulse (right column). Excitation signals transmitted to the cMUT are displayed in (a) and (b) while the resulting acoustic waveforms for a bias voltage of 90V are given in (c) and (d). Strong nonlinear distortions are visible in both acoustic waveforms. The cMUT nonlinear response depends on the transmit frequency and the distortions decrease with increasing the signal frequency (Lohfink and Eccardt 2005a). Corresponding spectra are shown in (e) and (f). For the sinusoidal burst, the 2^{nd} harmonic level is 10 dB below the fundamental while this value increases up to 8 dB for up-sweep frequency chirp. Although both excitation signals have the same amplitude and bandwidth, the transmission of chirped pulse results in more harmonic distortions. A quasi-similar level of 2^{nd} harmonic (± 0.8 dB) was measured when lower bias voltages (30V and 60V) were delivered (data not shown). On the contrary, for both the sinusoidal burst and chirped pulse, the level of the fundamental component, which depends on the bias voltage, was reduced by 3.6 ± 0.2 dB and 9.2 ± 0.4 dB for V_{dc}=60V and V_{dc}=30 V, respectively.

Axial resolution was calculated from the hydrophone measurements for both the sinusoidal burst and chirp excitations (Table III). The use of a compression filter reduced chirp lengths by a factor 2.1 and 1.8 at −3 dB and −20 dB, respectively. As a result, a quasi-similar axial resolution at −3 dB was achieved as compared to the sinusoidal burst (+0.08 mm).

Concurrently, the axial resolution at −20 dB for the compressed chirp still suffers from a slight degradation (+0.56 mm). This deterioration was attributed to a less efficient compression of the 2nd harmonic component generated by the cMUT.

B) Simulated response of a microbubble

The acoustic waveforms measured previously were introduced in the modified Rayleigh-Plesset equation as excitation signals. For each pulse, the simulated response from a microbubble was calculated and post-processing operations, corresponding to the different multi-pulse sequences (Table II), were applied to estimate the resulting signal (Figure 3). For all sequences, the resulting signal is nonzero and strongly asymmetric, revealing thus the presence of a high degree of nonlinearity in the microbubble responses. We assume these nonlinear distortions only correspond to the microbubble acoustic signature, as the undesirable signal generated by the cMUT is strongly reduced by BVM approach (Novell *et al* 2014a). The combination of BVM with PI results in a substantial increase of the resulting signal amplitude as PI emphasizes the amplitude of the 2nd harmonic response from microbubbles (Simpson *et al* 1999). This harmonic contribution is added to the nonlinear components (fundamental and 2nd harmonic) induced by BVM (Novell *et al* 2014a) and enhances the microbubble response. A similar trend is observed when BVMCR is combined with PI.

C) In vitro evaluation of the BVM sequence

The efficacy of each method in suppressing linear reflections from the source was evaluated. Echoes from a solid reflector (100 μm wire) were measured and post-processing was performed for every sequence to acquire the resulting signal. Examples of post-processed responses are displayed in Figure 4 for tone burst and chirped pulse based techniques. High-amplitude residual signals are observed for PI (a), CR (b) and CRPI (not shown). These undesirable signals are attributed to linear reflections of the harmonic components generated by the cMUT. Originally, all these sequences were developed to suppress linear reflections from the media and preserve nonlinear echoes from only the microbubbles. However, the principle and the efficacy of these approaches are based on the fact that the transmitted signal is purely linear. In the case of the cMUT transducer, the nonlinear wave emitted by the source is also preserved after processing and therefore could mask responses from nonlinear reflectors (*e.g.*, microbubbles). This observation is confirmed by the normalized frequency responses displayed in (c) and (d) where a high level of the 2nd harmonic component is observed when PI, CR and CRPI sequences are transmitted. As expected, the residual signal from the linear reflection is considerably reduced when BVM-based sequences are implemented. Concretely, the cancellation of the 2nd harmonic is above 20 dB when BVM is combined with other approaches (*i.e.*, PI, CR, CRPI). Furthermore, a reduction of the fundamental component above 26 dB is achieved for every imaging method. The noise level is also considerably reduced when chirped sequences were used. These results demonstrate that BVM can be successfully combined with other approaches to efficiently cancel nonlinear signals generated by the source.

Responses from microbubbles circulating in the microcellulose tube were used to quantify the sensitivity of the evaluated sequences. The contrast enhancement in Figure 5(a) and

CNR in Figure 5(b) reported here are mean values ± standard error of mean (SEM) and were determined from three independent measurements. For contrast enhancement, each result was normalized to the echoes received from the linear reflector control experiments (100 μm wire). A significant contrast enhancement of 18.6 dB is achieved for BVMCRPI. Compared with CRPI and BVM, the contrast is 14.2 dB and 5.5 dB higher, respectively. Concurrently, compared with BVM, the CNR is enhanced by 29.3 dB by combining BVM with CRPI. This is explained by the increase of the signal intensity received from microbubbles (Figure 3) and because more energy was transmitted with the chirped sequences.

In addition, comparison in terms of CTR enhancement was performed by measuring the received echoes from microbubbles circulating in a tube embedded in a tissue mimicking phantom. As expected, a better CTR (up to 8 dB) was measured for multi-pulse sequences involving the BVM scheme (Figure 6). As shown in Figure 4, this increase is attributed to a better suppression of the nonlinear component (emitted by the source) contained in the tissue response. Although the best CTR is measured for the BVMCR sequence, no significant differences are observed between BVM-based methods.

IV. DISCUSSION

The results from this study demonstrate that the combination of BVM approach with other imaging sequences presents two advantages. Firstly, the undesirable nonlinear components from cMUT, which are preserved when PI and CR are implemented, can be successfully compensated for when those approaches are associated with BVM. Secondly, our results suggest that contrast agent detection can be optimized by combining BVM with other imaging sequences. In fact, as shown in Figure 5, both contrast enhancement and CNR increased when BVMCRPI was implemented. These enhancements can be attributed to a better conservation of the different nonlinear components induced by each of BVM, CR and PI method. Indeed, this multi-pulse technique exploits different specific sources of nonlinearity generated in the microbubble response. Specifically, the PI sequence is known to enhance even harmonic responses (mainly the $2f_0$) of the contrast agent while suppressing the odd harmonic components, including the linear fundamental response (Simpson *et al* 1999). For the BVM sequence, as well as PM imaging, the level of nonlinear components is modified during amplitude modulation. At low acoustic pressures, the microbubble response is primarily linear and the harmonic amplitude remains weak, whereas at higher pressures, the generation of strong harmonics induces a loss of energy at the fundamental frequency. This specific property of microbubbles is used to discriminate the contrast agent responses from the surrounding media in the final image. The resulting signal after BVM processing is then composed by a nonlinear fundamental component (at f_0) and harmonic components (*i.e.*, $2f_0$, $3f_0$…) (Novell *et al* 2014a). For its part, CR imaging exploits the microbubble resonance phenomenon to generate different nonlinear vibrations according to the sign (x_{upf} *or* x_{dnf}) of the frequency sweep of the two chirps. Consequently, the resulting microbubble response is also composed of different frequencies (*e.g.*, f_0, $2f_0$) (Novell *et al* 2009b). For BVMCRPI, these different nonlinear sources (*i.e.*, from pulse inversion, amplitude modulation and resonance phenomenon) are accumulated and induce a further enhancement of nonlinear contrast agent responses. These findings agree well with previous studies

reporting CNR and CTR enhancements when PI is combined with PM (Eckersley *et al* 2005, Novell *et al* 2014b) or CR with PM (Novell *et al* 2014b).

Surprisingly, no significant differences were observed for BVM-based approaches when these sequences were evaluated using the tube embedded in the tissue mimicking phantom (Figure 6). This can be attributed to a higher attenuation of the high frequency components in the phantom (1.97 $dB.cm^{-1}$ at 4 MHz and 4.5 $dB.cm^{-1}$ at 8 MHz) reducing thus the level of the nonlinear components in the received responses. As a result, the contribution of both CR and PI approaches is probably too weak to induce a significant CTR enhancement. An enhancement of the CTR is expected using higher pressure amplitudes (mechanical index [0.1-0.5]) because of the accumulation of CR and PI nonlinear components are expected to increase relative to tissue nonlinear components.

As shown in Figs. 3 and 5b, the residual signal for BVM is quite low as compared to the other approaches. In the current study, the maximal pressure amplitude was limited by the sensitivity of the cMUT (operating in its conventional regime) and by the use of only 9 inter-connected elements in transmit. The relatively low transmit pressure (mechanical index ≤ 0.05) serves as a restriction and may have limited the contrast enhancement provided by BVM. At low pressures, microbubble oscillations are primarily linear. At higher pressures, the level of nonlinear distortion in responses of microbubbles is increased (de Jong *et al* 2002) and would likely make the method more efficient for contrast agent detection. In future work, this problem of sensitivity could be easily addressed by adding more elements to the cMUT array and by focusing the ultrasound beam. Furthermore, the BVM method was implemented using the voltage coefficients (*i.e.*, voltage ratios: 1,2,3) previously defined in (Novell *et al* 2014a). Nevertheless, we believe that an optimization in BVM coefficients (e.g., use of higher bias voltages) could be performed to improve the sensitivity of the approach.

Although the reduction of linear reflections was satisfactory (*i.e.*, −26 dB at f_0 and −15 dB at 2 f_0) for each sequence involving BVM, a complete cancellation of the nonlinear signal from the source was not achieved for combined approaches as shown in Figure 4. The presence of this residual signal is most likely due to the cMUT partially operating in the pre-collapse regime ($V_{dc}+v_{ac}$ close to the collapse voltage) when the highest V_{dc} voltage (*i.e.*, 90V) was transmitted. Furthermore, as only 9 elements of the prototype probe were available, it was necessary to apply a high excitation voltage (75 V_p) in order to increase the sensitivity of the probe. In these conditions, the dynamic collapse of the cMUT membrane could occur and generate additional nonlinearities. Indeed, it has been previously demonstrated that BVM is more efficient when the cMUT is used in its conventional operation regime (*i.e.*, $V_{dc}+v_{ac} << V_{collapse}$) (Novell *et al* 2014a). In this operation mode, the fundamental component increases linearly while the 2nd harmonic emitted by the cMUT remains quasi-constant as V_{dc} increases. On the contrary, when the probe is operated in the pre-collapse regime, both the fundamental and the second harmonic components considerably increase (Novell *et al* 2014a). This imperfect nonlinear cancellation can be considered as a limitation of our study but we believe that lower voltages can be applied using a full size cMUT transducer (128-elements) to reduce the cMUT nonlinearity.

As shown in Figure 2(d) for up-sweep frequency chirped pulse, nonlinearities are more important at the beginning of the waveform when low frequencies are transmitted. Similar phenomenon occurs when down-sweep frequency chirps are used. In that case, nonlinearities are more important at the end of the waveform (*i.e.*, for the transmission of low frequency components). As a consequence, nonlinearities are not generated at the same time for both chirps used in CR sequence. This behavior is illustrated in Figure 7a where the envelopes of the 2^{nd} harmonic components generated during chirped excitations are displayed. The delay between harmonic components is preserved after chirp compression (Figure 7b), making CR post-processing inefficient for harmonic suppression, as shown in Figure 4d where a substantial 2^{nd} harmonic response (at 7.2 MHz and 8.5 MHz) from a linear reflector is measured. It is noticeable that, at exactly 8 MHz, a good cancellation of the nonlinear response was found because this harmonic frequency ($2f_0$) was generated at the center of both chirps. One option to suppress the delay between both harmonic responses (approximately 0.2 μs in this study) would consist in adjusting the compression filters. However, as this delay mainly depends on the intrinsic properties of the cMUT and chirp excitation parameters (*e.g.*, frequency sweep), compression filters should be adapted for each specific circumstance. Therefore, a non restricted option consisting in the transmission of four firings (2 x_{upf} and 2 x_{dnf}) was chosen as shown in Table I. Here, nonlinearities were compensated by subtracting up-sweep frequency chirps from each other (E_1 and E_3 should have opposite sign), and by doing the same operation for down-sweep frequency chirps (E_2 and E_4 should have opposite sign). Consequently, a trade-off between improving the contrast agent detection (Figure 5b) and reducing the frame rate has to be considered when CR is combined with BVM.

Although the axial resolution given for chirped excitation in Table III is correct for CR, the result may be overestimated for BVMCR-based sequences. Originally, the compression filter used in this study was specifically designed to extract the nonlinear responses from microbubbles (at f_0 and $2f_0$) while limiting side lobe artifacts induced during compression (Novell *et al* 2014b). Nevertheless, the 2^{nd} harmonic component generated by the cMUT has a specific bandwidth and phase dependent on the cMUT characteristics and the compression filter was not adapted for this harmonic component. As a result, the compression of this chirped wave containing this undesirable 2^{nd} harmonic component is not optimal and results in a slight degradation of the axial resolution. However, as cMUT nonlinearities are suppressed for BVMCR-based sequences, we believe that the axial resolution may be improved over the results given in Table III.

V. CONCLUSIONS

The results of this study demonstrate that contrast agent detection can be improved by combining a bias voltage modulation sequence with pulse inversion and chirp reversal. Indeed, the use of a chirped pulse resulted in a significant increase in CNR because more energy was transmitted in the excitation signal. In addition, the contrast enhancement is attributed to the contribution of the different nonlinear components (*i.e.*, nonlinear fundamental and 2^{nd} harmonic) simultaneously induced by BVM, PI and CR. The wideband compression filter used in this study was specifically designed to recover these frequency components. Nevertheless, the significant gain in sensitivity is contrasted by a slight

degradation of the axial resolution as compared to sinusoidal pulse excitation, and a limited frame rate as 4 firings are required to efficiently suppress the cMUT nonlinear behavior. Further investigations will involve the implementation of BVMCRPI imaging on a research ultrasound scanner and *in vivo* validation of the sequence. Furthermore, we believe that this sequence which exploits the wide bandwidth of a cMUT transducer could be applied to superharmonic imaging.

ACKNOWLEDGEMENTS

The authors thank Vermon (Tours, France) for providing the cMUT transducers used in the work described here. We also thank Dr. Jean-Marc Gregroire (Inserm U930, University of Tours, France) for technical assistance, Dr. Jean-Michel Escoffre (UMC, Utrecht, the Netherlands) for statistical analysis and Dr. Brooks L. Lindsey (The University of North Carolina, Chapel Hill, USA) for fruitful discussion. A. Novell gratefully acknowledge the foundation ARC (n°SAE20130606511) for financial support. C.B. Arena acknowledges support from a grant from the National Institute of General Medical Sciences, division of Training, Workforce Development, and Diversity under the Institutional Research and Academic Career Development Award, grant #K12-GM000678.

REFERENCES

Bayram B, Oralkan O, Ergun AS, Haeggstrom E, Yaralioglu GG, Khuri-Yakub BT. Capacitive micromachined ultrasonic transducer design for high power transmission. IEEE Trans Ultrason Ferroelectr Freq Control. 2005; 52:326–39. [PubMed: 15801320]

Borsboom JM, Chin CT, Bouakaz A, Versluis M, De Jong N. Harmonic chirp imaging method for ultrasound contrast agent. IEEE Trans Ultrason Ferroelectr Freq Control. 2005; 52:241–9. [PubMed: 15801312]

Bouakaz A, Frigstad S, Ten Cate FJ, De Jong N. Super harmonic imaging: a new imaging technique for improved contrast detection. Ultrasound Med Biol. 2002; 28:59–68. [PubMed: 11879953]

Brock-Fisher, G.; Poland, M.; Rafter, P. Means for increasing sensitivity in non-linear ultrasound imaging systems. USA patent application 5577505A. 1996.

Chen J, Wang M, Cheng JC, Wang YH, Li PC, Cheng X. A photoacoustic imager with light illumination through an infrared-transparent silicon CMUT array. IEEE Trans Ultrason Ferroelectr Freq Control. 2012; 59:766–75. [PubMed: 22547287]

Chomas J, Dayton P, May D, Ferrara K. Nondestructive subharmonic imaging. IEEE Trans Ultrason Ferroelectr Freq Control. 2002; 49:883–92. [PubMed: 12152942]

De Jong N, Bouakaz A, Frinking P. Basic acoustic properties of microbubbles. Echocardiography. 2002; 19:229–40. [PubMed: 12022933]

De Jong N, Cornet R, Lancee CT. Higher harmonics of vibrating gas filled microspheres. Part one: Simulations. Ultrasonics. 1994; 32:447–453.

Eckersley RJ, Chin CT, Burns PN. Optimising phase and amplitude modulation schemes for imaging microbubble contrast agents at low acoustic power. Ultrasound Med Biol. 2005; 31:213–9. [PubMed: 15708461]

Frinking PJ, Bouakaz A, Kirkhorn J, Ten Cate FJ, De Jong N. Ultrasound contrast imaging: current and new potential methods. Ultrasound Med Biol. 2000; 26:965–75. [PubMed: 10996696]

Gessner RC, Frederick CB, Foster FS, Dayton PA. Acoustic angiography: a new imaging modality for assessing microvasculature architecture. Int J Biomed Imaging. 2013; 2013:936593. [PubMed: 23997762]

Goertz DE, De Jong N, Van Der Steen AF. Attenuation and size distribution measurements of Definity and manipulated Definity populations. Ultrasound Med Biol. 2007; 33:1376–88. [PubMed: 17521801]

Hamilton, M.; Blackstock, D. Nonlinear acoustics. Academic; San Diego, CA: 1998. p. 455

Huang Y, Haeggstrom E, Bayram B, Zhuang X, Ergun AS, Cheng CH, Khuri-Yakub BT. Comparison of conventional and collapsed region operation of capacitive micromachined ultrasonic transducers. IEEE Trans Ultrason Ferroelectr Freq Control. 2006; 53:1918–33. [PubMed: 17036801]

Ignee A, Straub B, Schuessler G, Dietrich CF. Contrast enhanced ultrasound of renal masses. World J Radiol. 2010; 2:15–31. [PubMed: 21160736]

King RL, Liu YB, Maruvada S, Herman BA, Wear KA, Harris GR. Development and Characterization of a Tissue-Mimicking Material for High-Intensity Focused Ultrasound. Ieee Transactions on Ultrasonics Ferroelectrics and Frequency Control. 2011; 58:1397–1405.

Lohfink, A.; Eccardt, PC. Investigation of nonlinear CMUT behavior; Proc. IEEE Ultrasonics symposium; 2005a; p. 585-588.

Lohfink A, Eccardt PC. Linear and nonlinear equivalent circuit modeling of CMUTs. IEEE Trans Ultrason Ferroelectr Freq Control. 2005b; 52:2163–72. [PubMed: 16463483]

Madsen EL, Dong F, Frank GR, Garra BS, Wear KA, Wilson T, Zagzebski JA, Miller HL, Shung KK, Wang SH, Feleppa EJ, Liu T, O'brien WD, Topp KA, Sanghvi NT, Zaitsev AV, Hall TJ, Fowlkes JB, Kripfgans OD, Miller JG. Interlaboratory comparison of ultrasonic backscatter, attenuation, and speed measurements. Journal of Ultrasound in Medicine. 1999; 18:615–631. [PubMed: 10478971]

Maresca D, Renaud G, Van Soest G, Li X, Zhou Q, Shung KK, De Jong N, Van Der Steen AF. Contrast-enhanced intravascular ultrasound pulse sequences for bandwidth-limited transducers. Ultrasound Med Biol. 2013; 39:706–13. [PubMed: 23384459]

Misaridis T, Jensen JA. Use of modulated excitation signals in medical ultrasound. Part I: Basic concepts and expected benefits. IEEE Trans Ultrason Ferroelectr Freq Control. 2005; 52:177–91. [PubMed: 15801307]

Misaridis TX, Gammelmark K, Jorgensen CH, Lindberg N, Thomsen AH, Pedersen MH, Jensen JA. Potential of coded excitation in medical ultrasound imaging. Ultrasonics. 2000; 38:183–9. [PubMed: 10829655]

Mullin L, Gessner R, Kwan J, Kaya M, Borden MA, Dayton PA. Effect of anesthesia carrier gas on in vivo circulation times of ultrasound microbubble contrast agents in rats. Contrast Media Mol Imaging. 2011; 6:126–31. [PubMed: 21246710]

Mulvagh SL, Demaria AN, Feinstein SB, Burns PN, Kaul S, Miller JG, Monaghan M, Porter TR, Shaw LJ, Villanueva FS. Contrast echocardiography: current and future applications. J Am Soc Echocardiogr. 2000; 13:331–42. [PubMed: 10756254]

Novell A, Escoffre JM, Bouakaz A. Second harmonic and subharmonic for non-linear wideband contrast imaging using a capacitive micromachined ultrasonic transducer array. Ultrasound Med Biol. 2013a; 39:1500–12. [PubMed: 23743105]

Novell A, Escoffre JM, Bouakaz A. Ultrasound contrast imaging in cancer – Technical aspects and prospects. Current Molecular Imaging. 2013b; 2:77–88.

Novell A, Legros M, Felix N, Bouakaz A. Exploitation of capacitive micromachined transducers for nonlinear ultrasound imaging. IEEE Trans Ultrason Ferroelectr Freq Control. 2009a; 56:2733–43. [PubMed: 20040410]

Novell A, Legros M, Gregoire JM, Dayton PA, Bouakaz A. Evaluation of bias voltage modulation sequence for nonlinear contrast agent imaging using a capacitive micromachined ultrasonic transducer array. Phys Med Biol. 2014a; 59:4879–96. [PubMed: 25098319]

Novell A, Sennoga CA, Escoffre JM, Chaline J, Bouakaz A. Evaluation of chirp reversal power modulation sequence for contrast agent imaging. Phys Med Biol. 2014b; 59:5101–17. [PubMed: 25122547]

Novell A, Van Der Meer S, Versluis M, De Jong N, Bouakaz A. Contrast agent response to chirp reversal: simulations, optical observations, and acoustical verification. IEEE Trans Ultrason Ferroelectr Freq Control. 2009b; 56:1199–206. [PubMed: 19574127]

O'donnell M. Coded excitation system for improving the penetration of real-time phased-array imaging systems. IEEE Transactions UFFC. 1992; 39:341–351.

Park J, Li X, Zhou Q, Shung KK. Combined chirp coded tissue harmonic and fundamental ultrasound imaging for intravascular ultrasound: 20-60 MHz phantom and ex vivo results. Ultrasonics. 2013; 53:369–76. [PubMed: 22871273]

Phillips, PJ. Contrast Pulse Sequences (CPS): imaging nonlinear microbubbles; Proc. IEEE Ultrasonics symposium; 2001; p. 1739-1745.

Pohlhammer, JD.; O'brien, WD, Jr.. The Relationship Between Ultrasonic Attenuation and Speed In Tissues and the Constituents: Water, Collagen, Protein, and Fat. Published for the American Association of Physicists in Medicine by the American Institute of Physics; New York: 1980.

Satir S, Degertekin FL. Harmonic reduction in capacitive micromachined ultrasonic transducers by gap feedback linearization. IEEE Trans Ultrason Ferroelectr Freq Control. 2012; 59:50–9. [PubMed: 22293735]

Savoia A, Calianov G, Pappalardo M. A CMUT probe for medical ultrasonography: from microfabrication to system integration. IEEE Trans Ultrason Ferroelectr Freq Control. 2012; 59:1127–38. [PubMed: 22711408]

Shekhar H, Doyley MM. The response of phospholipid-encapsulated microbubbles to chirp-coded excitation: Implications for high-frequency nonlinear imaging. J Acoust Soc Am. 2013; 133:3145–58. [PubMed: 23654417]

Shin M, Krause JS, Debitetto P, White RD. Acoustic Doppler velocity measurement system using capacitive micromachined ultrasound transducer array technology. J Acoust Soc Am. 2013; 134:1011–20. [PubMed: 23927100]

Simpson D, Chin C, Burns P. Pulse inversion Doppler: A new method for detecting nonlinear echoes from microbubble contrast agents. IEEE Trans Ultrason Ferr Freq Con. 1999; 46:372–382.

Song J, Chang JH, Song TK, Yoo Y. Coded tissue harmonic imaging with nonlinear chirp signals. Ultrasonics. 2011; 51:516–21. [PubMed: 21216422]

Tekes C, Zahorian J, Gurun G, Satir S, Xu T, Hochman M, Degertekin FL. Volumetric imaging using single chip integrated CMUT-on-CMOS IVUS array. Conf Proc IEEE Eng Med Biol Soc. 20122012:3195–8. [PubMed: 23366605]

Vaithilingam S, Ma TJ, Furukawa Y, Wygant IO, Zhuang X, De La Zerda A, Oralkan O, Kamaya A, Gambhir SS, Jeffrey RB Jr. Khuri-Yakub BT. Three-dimensional photoacoustic imaging using a two-dimensional CMUT array. IEEE Trans Ultrason Ferroelectr Freq Control. 2009; 56:2411–9. [PubMed: 19942528]

Wilson SR, Burns PN. Microbubble-enhanced US in body imaging: what role? Radiology. 2010; 257:24–39. [PubMed: 20851938]

Wong SH, Kupnik M, Watkins RD, Butts-Pauly K, Khuri-Yakub BT. Capacitive micromachined ultrasonic transducers for therapeutic ultrasound applications. IEEE Trans Biomed Eng. 2010; 57:114–23. [PubMed: 19628448]

Zhang D, Gong Y, Gong X, Liu Z, Tan K, Zheng H. Enhancement of subharmonic emission from encapsulated microbubbles by using a chirp excitation technique. Phys Med Biol. 2007; 52:5531–44. [PubMed: 17804880]

Zhou S, Reynolds P, Hossack J. Precompensated excitation waveforms to suppress harmonic generation in MEMS electrostatic transducers. IEEE Trans Ultrason Ferroelectr Freq Control. 2004; 51:1564–74. [PubMed: 15600102]

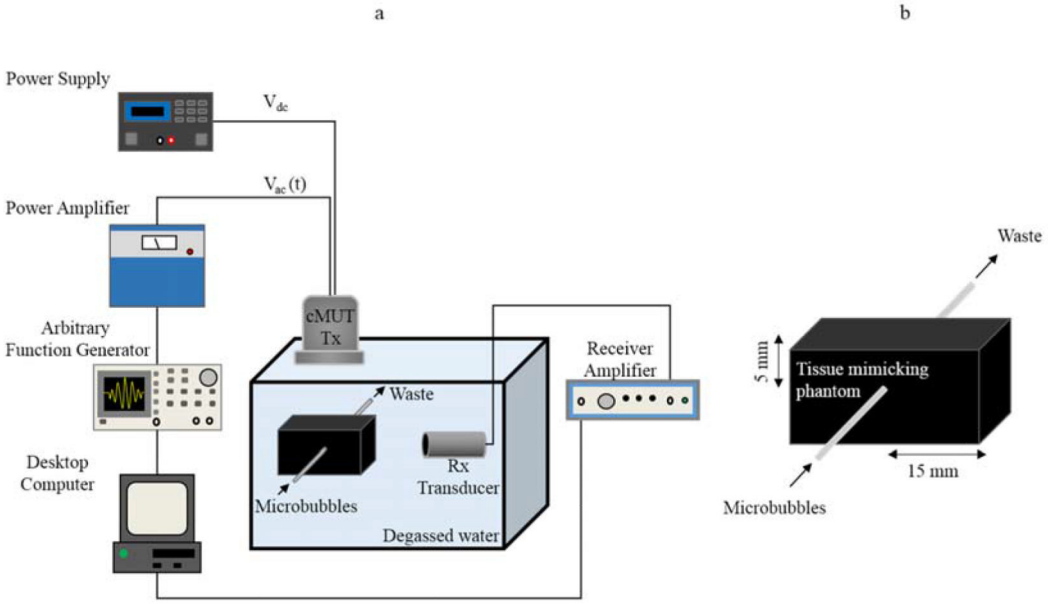

Figure 1.
Experimental setup used for the *in vitro* measurements (a). Tissue mimicking phantom (b).

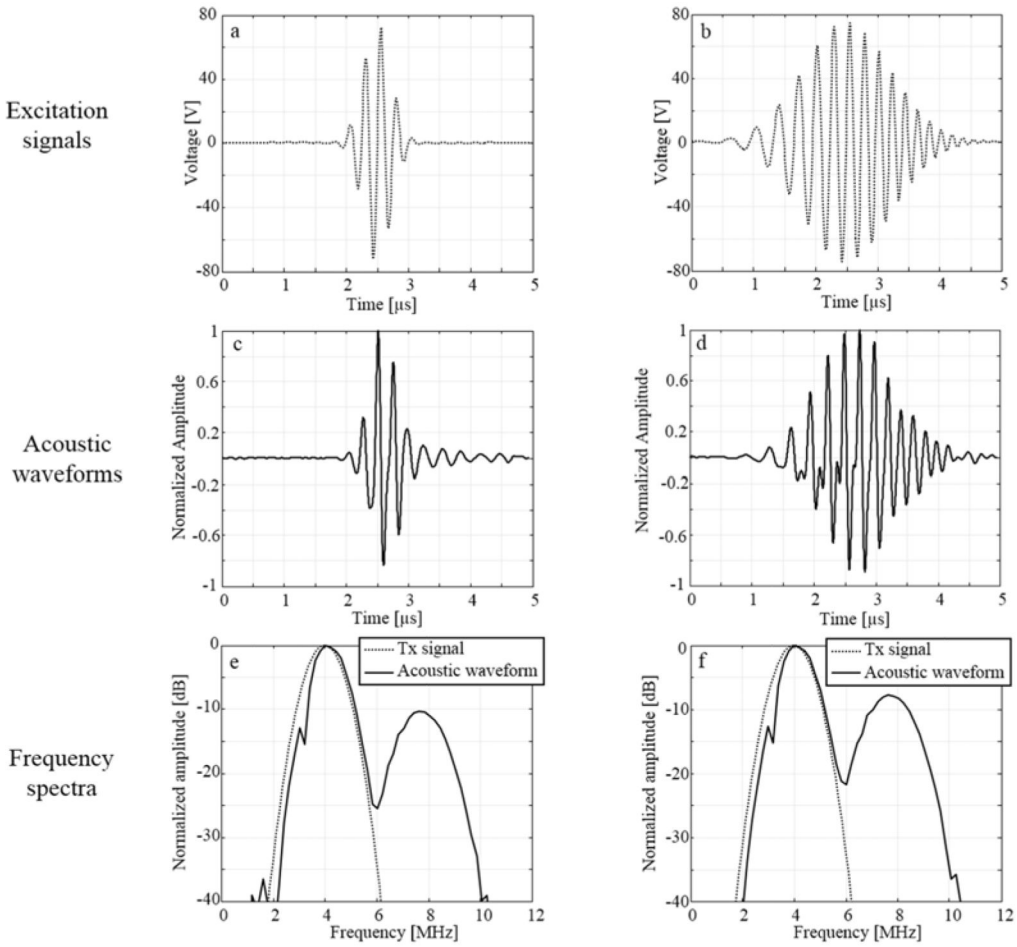

Figure 2.

Examples of Gaussian pulse x_p (a) and up-sweep frequency chirp x_{upf} (b) signals transmitted to the cMUT. Hydrophone measurements in the vicinity of the cMUT surface of acoustic waveforms resulting from x_p and x_{upf} are given in (c) and (d). Corresponding spectra are shown in (e) and (f), for the pulse and the chirp signals, respectively.

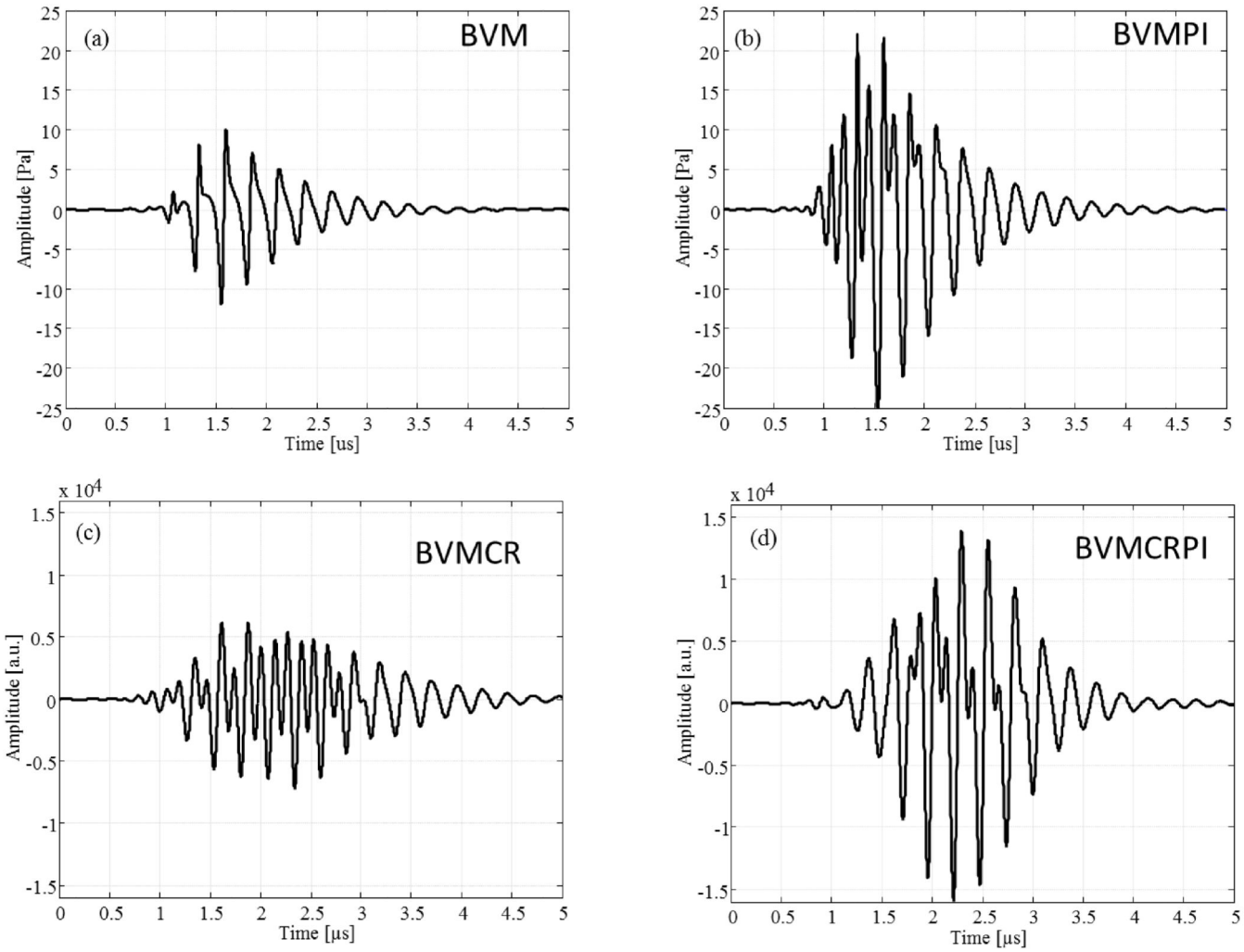

Figure 3.

Resulting responses of a simulated contrast microbubble with radius 1.3 μm for BVM (a), BVMPI (b), BVMCR (c) and BVMCRPI (d) approaches.

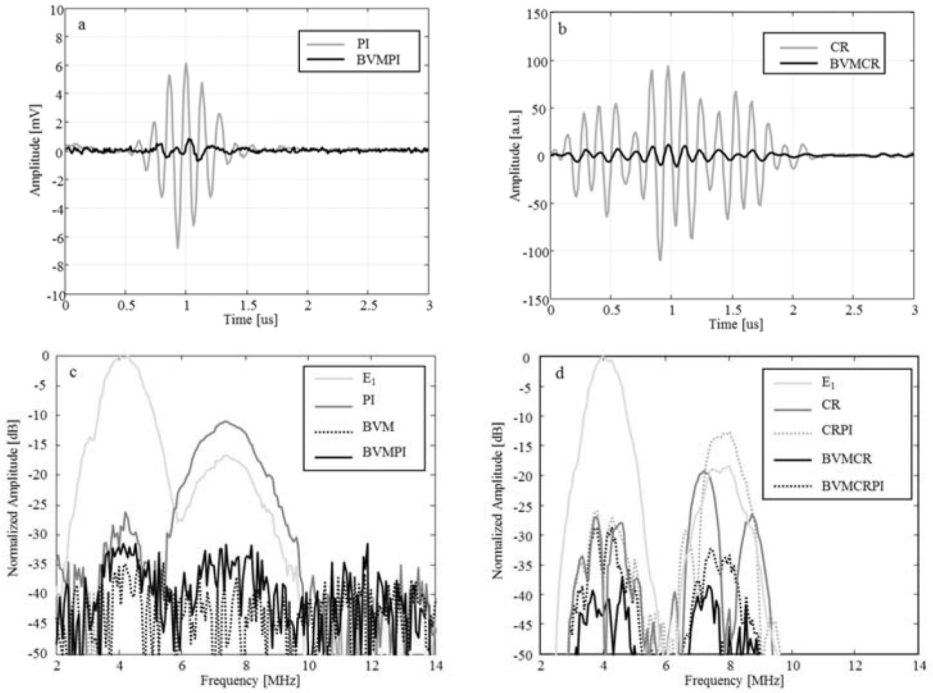

Figure 4.

Examples of residual responses from a linear reflector (100 μm diameter wire) after processing for PI and BVMPI (a); CR and BVMCR (b). Spectra of the residual responses after processing are given for multi-pulse sequences based on pulse (c) and chirp (d) excitations.

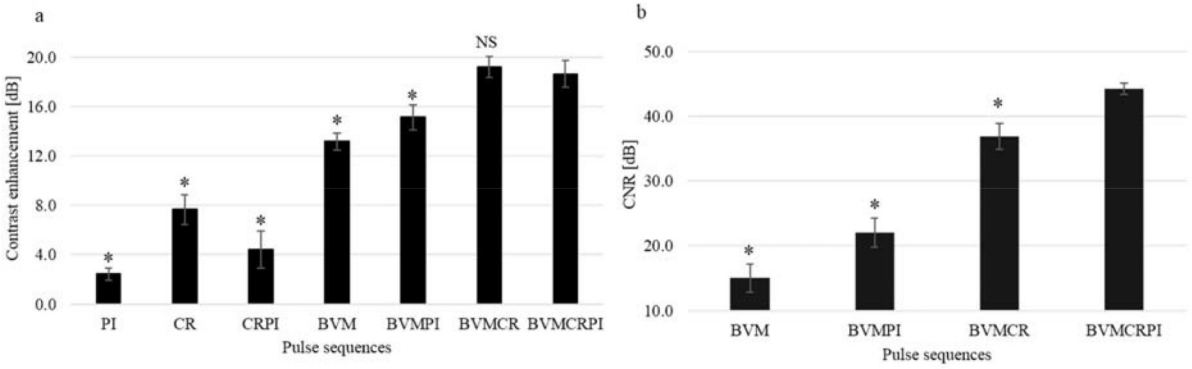

Figure 5.

Contrast enhancement (a) and CNR (b) as a function of contrast imaging approach implemented. For contrast enhancement measurements, each result was normalized to the echoes received from the linear scatterer experiment (100 μm diameter wire). Statistical analysis was performed using the nonparametric experiments Mann–Whitney test. Significance was defined as * $p<0.05$ compared to BVMCRPI (NS, non significant).

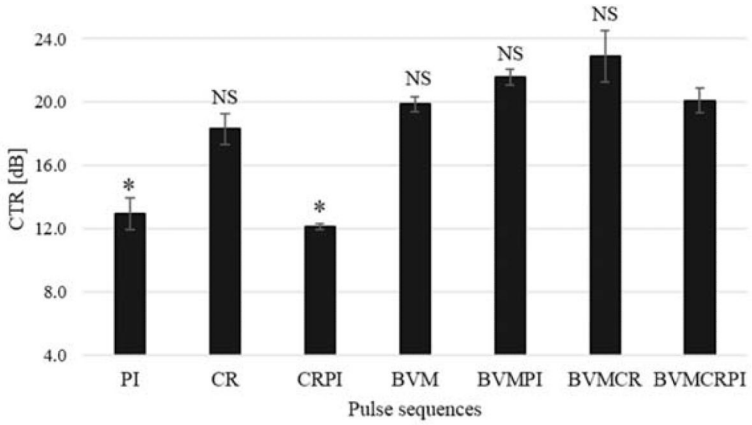

Figure 6.

CTR measurements as a function of contrast imaging approach. Statistical analysis was performed using the nonparametric experiments Mann–Whitney test. Significance was defined as * $p<0.05$ compared to BVMCRPI (NS, non significant).

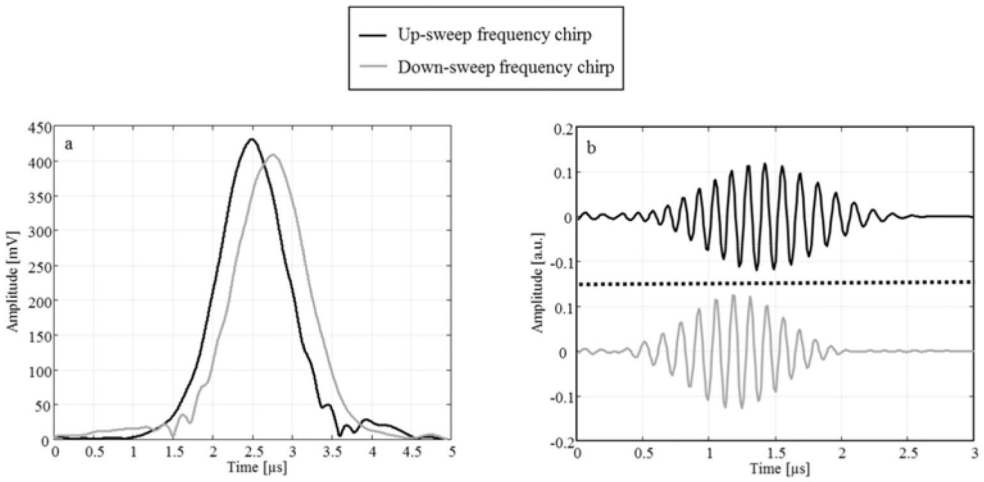

Figure 7.

Envelopes of the second harmonic components for up-sweep frequency chirp x_{upf} and down-sweep frequency chirp x_{dnf} (a). Harmonic signals after compression (b).

Table I

List of the transmitted excitation signals as a function of the contrast imaging sequence.

Contrast imaging sequence	PI	CR	CRPI	BVM	BVMPI	BVMCR	BVMCRPI
First excitation signal (s_1)	x_p	x_{upf}	x_{upf}	x_p	x_p	x_{upf}	x_{upf}
Second excitation signal (s_2)	$-x_p$	x_{dnf}	$-x_{dnf}$	x_p	$-x_p$	x_{upf}	$-x_{dnf}$
Third excitation signal (s_3)				x_p	x_p	x_{upf}	x_{upf}
Fourth excitation signal (s_4)						x_{dnf}	x_{dnf}

x_p: pulse

x_{upf}: up-sweep frequency chirp

x_{dnf}: down-sweep frequency chirp

V_{dc} = 30V

V_{dc} = 60V

V_{dc} = 90V

Table II

Examples of post-processing combinations required to suppress the linear scattering from echoes.

Contrast imaging sequence	PI	CR	CRPI	BVM	BVMPI	BVMCR	BVMCRPI
Post-processing operation	E_1+E_2	E_1-E_2	E_1+E_2	$0.75\ E_1+0.75\ E_3-1.5\ E_2$	$E_1+(2/3)\ E_2-(5/3)\ E_3$	$(3/7)\ E_1+(6/7)\ E_2$ $-(3/7)\ E_3-(6/7)\ E_4$	$E_1+(2/5)\ E_2$ $-E_3-(2/5)\ E_4$

Table III

Axial resolution obtained from hydrophone measurements using pulse and chirp excitations.

	Pulse	Chirp without compression	Chirp after compression
Axial resolution at −3 dB [mm]	0.50	1.24	0.58
Axial resolution at −20 dB [mm]	1.59	3.84	2.15